Title

Models Of Vehicular Collision: Development And Simulation With Emphasis On Safety II: On The Modeling Of Collision Between Vehicles In A Platoon System

Authors

O'reilly, Oliver M.
Et. al.

Publication Date

1997

CALIFORNIA PATH PROGRAM
INSTITUTE OF TRANSPORTATION STUDIES
UNIVERSITY OF CALIFORNIA, BERKELEY

Models of Vehicular Collision: Development and Simulation with Emphasis on Safety II: On the Modeling of Collision between Vehicles in a Platoon System

Oliver M. O'Reilly, Panayiotis Papadopoulos,
Gwo-Jeng Lo, Peter C. Varadi

California PATH Research Report
UCB-ITS-PRR-97-34

This work was performed as part of the California PATH Program of the University of California, in cooperation with the State of California Business, Transportation, and Housing Agency, Department of Transportation; and the United States Department of Transportation, Federal Highway Administration

July 25, 1997
ISNN 1055-1425

Models of Vehicular Collision: Development and Simulation with Emphasis on Safety
II: On the Modeling of Collision between Vehicles in a Platoon System

REPORT – July 1997

Submitted to: PATH (MOU 232)

Oliver M. O'Reilly (PI)
Panayiotis Papadopoulos (PI)
Gwo-Jeng Lo
Peter C. Varadi

Department of Mechanical Engineering
University of California, Berkeley

Abstract

In this report, an algorithm for the detection of collision between two vehicles is presented. The mechanical models used for the vehicles are based on the theory of a Cosserat point. Here, we find it convenient to establish the corresponding models using the theory of a pseudo-rigid body. This theory facilitates the development of our collision-detection algorithm. The report concludes with four examples of vehicular impact scenarios in order to illustrate the applicability of the proposed algorithm.

Keywords: IVHS America, Vehicle Dynamics, Collision Dynamics, Safety, Computer Simulation, Animation and Simulation

Executive Summary

In the companion report (O'Reilly, Papadopoulos, Lo and Varadi [19]), a model was developed for a single vehicle based on the theory of a Cosserat point. This model was intended as a predictive tool for vehicle simulations at low relative collision speeds. To use this model, it is necessary to develop the capabilities to detect possible collisions between two vehicles which are modeled using the formulation in [18]. The focus of the present report is the development of a collision-detection algorithm which can be used for this purpose.

To develop the collision-detection algorithm, we find it convenient to employ the theory of a pseudo-rigid body due to Cohen and Muncaster, and it can easily be placed in correspondence with the theory of a Cosserat point. Consequently, the algorithm developed in this report can be used with our earlier vehicle model.

The report begins with a summary of the theory of a pseudo-rigid body. For convenience, we also relate this theory to the more familiar theories of rigid bodies and classical continua. After this summary, an approximate model of the vehicles' geometries is developed. This model approximates each vehicle as a pseudo-rigid (deformable) ellipsoid. Due to the spatially homogeneous deformation undergone by the pseudo-rigid body, these ellipsoids remain ellipsoids in any subsequent elastic deformation. The surface of these bodies is parameterized by two coordinates, and the collision-detection algorithm provides the points of impact between them. This information is subsequently used in conjunction with the vehicular model to predict the post-collision response of the vehicles.

To illustrate the algorithm, selected examples are presented and discussed. The examples pertain to pseudo-rigid bodies where some of the features of the vehicle model have been ignored: this was necessary in order to validate the predictive capabilities of the algorithm. In the future, we intend to incorporate the algorithm with the vehicular model that was developed in [19] in order to simulate the collision of several vehicles.

Contents

0.1 Introduction

In the companion report (O'Reilly, Papadopoulos, Lo and Varadi [19]), a model was developed for a single vehicle based on the theory of a Cosserat point. This model was intended as a predictive tool for vehicle simulations at low relative collision speeds. To use this model it is necessary to develop the capabilities to detect possible collisions between two vehicles which are modeled using the formulation in [19]. The focus of the present report is the development of a collision-detection algorithm which can be used for this purpose.

In the preceding report, the theory of a Cosserat point was used to establish a vehicular model. However, to facilitate the development of the collision-detection algorithm, we find it easier to employ the theory of a pseudo-rigid body. This theory was developed by Cohen [6] and Muncaster [10] in the 1980's. A related theory was also developed, somewhat earlier, by Slawianowski (see [23], [24] and [25]). Briefly, the pseudo-rigid body is a deformable continuum capable of undergoing only homogeneous deformation. The theory of a Cosserat point, which was developed by Rubin and Green and Naghdi (see [12], [21] and [22]), can be placed in direct correspondence to the theory of a pseudo-rigid body. Hence, the developments of this report are applicable to the vehicle model discussed in [19]. The reader is referred to this report for a comprehensive discussion of the computational advantages of the vehicle models used here when compared with traditional methods.

This report begins with a summary of the theory of a pseudo-rigid body, which is presented in Section 2. For convenience, we also relate this theory to the more familiar theories of rigid bodies and classical continua. After this summary, an approximate model of the vehicles' geometries is developed in Section 3. This model approximates each vehicle as a pseudo-rigid (deformable) ellipsoid. Due to the deformation captured by the pseudo-rigid body, these ellipsoids remain ellipsoids in any subsequent deformation. The surface of these ellipsoids is parameterized by two coordinates, and the collision-detection algorithm provides the points of impact of the ellipsoids. This information is subsequently used in conjunction with the vehicular model to predict the post-collision response of the vehicles.

To illustrate the algorithm, selected examples are presented and discussed in Section 4. The examples pertain to pseudo-rigid bodies where some of the features of the vehicle model have been ignored: this was necessary in order to validate the predictive capacity of the algorithm. In the

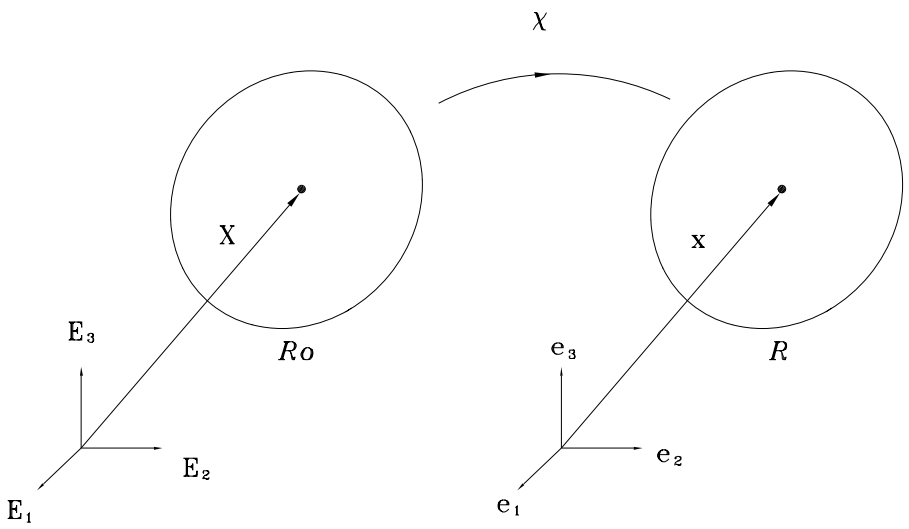

Figure 0.1: The reference and current configuration of body $\mathcal{B}$.

future, we intend to incorporate the algorithm with the vehicular model that was developed in [19] in order to simulate the collision of several vehicles.

0.2 Introduction to Pseudo-rigid Bodies

0.2.1 Theory of Deformable Bodies

Consider a body $\mathcal{B}$ which at time t_o occupies a region $\mathcal{R}_o$ in the Euclidean three point space E^3, and is bounded by a smooth closed surface $\partial\mathcal{R}_o$. The same body at time t occupies a region $\mathcal{R}$ which is bounded by a closed surface $\partial\mathcal{R}$. Let $\mathbf{X}$ and $\mathbf{x}$ denote, respectively, the position vectors of a particle X in the reference configuration at time t_o and present configuration at time t, with respect to fixed orthonormal bases $\mathbf{E}_A$ and $\mathbf{e}_i$, respectively, as shown in Figure 1.

The motion $\boldsymbol{\chi}$ of the deformable body $\mathcal{B}$ is defined so that at time t,

$$\mathbf{x} \;=\; \boldsymbol{\chi}(\mathbf{X}, t)\;, \tag{0.1}$$

where $\boldsymbol{\chi}$ is assumed differentiable as many times as desired. The deformation

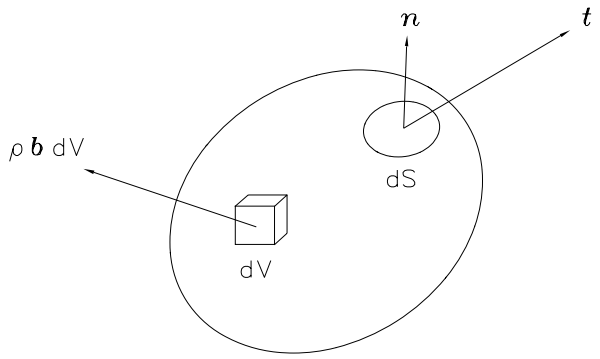

Figure 0.2: Momentum balance.

gradient relative to the reference configuration is defined by

$$\mathbf{F} \;=\; \frac{\partial \boldsymbol{\chi}(\mathbf{X},t)}{\partial \mathbf{X}} \;, \tag{0.2}$$

and its Jacobian J= det$\mathbf{F}$ is assumed to be non-zero for all t. The non-vanishing of J implies the existence of the inverse deformation gradient $\mathbf{F}^{-1}$ and also guarantees the invertibility of the motion described by (1).

Two types of external forces are admitted, namely body forces $\mathbf{b}$ per unit mass and surface forces (or contact forces) $\mathbf{t} = \mathbf{t}(\mathbf{X}, t; \mathbf{n})$ per unit area, where $\mathbf{n}$ denotes the outward unit normal to the surface, as shown in Figure 2. The three basic physical principles in the purely mechanical theory are conservation of mass, balance of linear momentum and balance of angular momentum [18]. The last two principles state that the total linear momentum and angular momentum of each part of the body are balanced in the sense that their rates of change are equal to the total applied force and torque, respectively. These are often referred to as Euler's laws. These laws have been applied successfully in both rigid-body and deformable-body mechanics. In the latter case, they lead to local forms usually referred to as Cauchy's first and second law, respectively.

The integral forms of the momentum balance laws for a part $\mathcal{S}$ of the body $\mathcal{B}$ occupying, in the current configuration, a region $\mathcal{P}$ with boundary surface $\partial\mathcal{P}$ are written as:

$$\frac{d}{dt}\int_{\mathcal{P}} \rho\mathbf{v}\; dv \;=\; \int_{\partial\mathcal{P}} \mathbf{t}\; da \;+\; \int_{\mathcal{P}} \rho\mathbf{b}\; dv = \mathbf{f}\;, \tag{0.3}$$

$$\frac{d}{dt}\int_{\mathcal{P}} \mathbf{x}\times\rho\mathbf{v}\ dv \ = \ \int_{\partial\mathcal{P}} \mathbf{x}\times\mathbf{t}\ da \ + \ \int_{\mathcal{P}} \rho\mathbf{x}\times\mathbf{b}\ dv = \mathbf{M}\ , \tag{0.4}$$

where $\mathbf{f}$ and $\mathbf{M}$, respectively, are the resultant external force vector and moment vector on $\partial\mathcal{P}$ with respect to the origin of the orthonormal basis $\mathbf{e}_i$. In addition, ρ is the mass density in the current configuration and $\mathbf{v}$ is the velocity vector.

A standard argument leads to Cauchy's theorem for the existence of the stress tensor: the stress vector $\mathbf{t}$ depends linearly on the normal $\mathbf{n}$, i.e., $\mathbf{t} = \mathbf{T}\mathbf{n}$, where $\mathbf{T}$ is the Cauchy stress tensor (also known as true stress). Upon application of the divergence theorem and Reynolds transport theorem, one obtains

$$\int_{\mathcal{P}} (\mathrm{div}\mathbf{T} \ + \ \rho\mathbf{b} \ - \ \rho\dot{\mathbf{v}})\ \mathrm{dv} = \mathbf{0}\ , \tag{0.5}$$

where $\mathrm{div}\mathbf{T} = \frac{\partial \mathrm{T_{ij}}}{\partial \mathrm{x_j}}\mathbf{e}_i$ and the summation convention is enforced for roman indices. Recalling the arbitrariness of $\mathcal{P}$ and using the localization theorem, it follows that

$$\mathrm{div}\mathbf{T} \ + \ \rho\mathbf{b} \ = \ \rho\dot{\mathbf{v}}\ , \tag{0.6}$$

which is Cauchy's first law of motion. Obviously, equation (6) is a *partial*differential equation. A similar procedure can be applied to equation (4), yielding Cauchy's second law of motion in the form

$$\mathbf{T} \ = \ \mathbf{T}^T\ . \tag{0.7}$$

0.2.2 Rigid Body Mechanics

A rigid body can only undergo a motion of the form

$$\mathbf{x} \ = \ \mathbf{Q}(t)\ \mathbf{X} \ + \ \mathbf{c}(t)\ , \tag{0.8}$$

where $\mathbf{Q}$ is a proper orthogonal tensor-valued function (namely, $\mathbf{Q}\mathbf{Q}^T = \mathbf{Q}^T\mathbf{Q} = \mathbf{I}$, where $\mathbf{I}$ is the identity tensor and $\det\mathbf{Q} = 1$) and $\mathbf{c}$ a vector-valued function, both depending on time only (cf. [3], [4] and [28]). The total mass of $\mathcal{B}$ is

$$m \ = \ \int_{\mathcal{R}} \rho\ dv \ = \ \int_{\mathcal{R}_o} \rho_o\ dV\ , \tag{0.9}$$

where ρ_o is the mass density in the reference configuration. Next, introduce the position vectors $\bar{\mathbf{X}}$ and $\bar{\mathbf{x}}$ of the mass center of the body in the reference and current configuration, respectively, as

$$m\bar{\mathbf{X}} \;=\; \int_{\mathcal{R}_o} \rho_o \mathbf{X}\; dV \;, \tag{0.10}$$

$$m\bar{\mathbf{x}} \;=\; \int_{\mathcal{R}} \rho \mathbf{x}\; dv \;. \tag{0.11}$$

Also, let the relative position vector in the reference configuration be defined as $\mathbf{\Pi} = \mathbf{X} - \bar{\mathbf{X}}$, such that

$$\int_{\mathcal{R}_o} \rho_o \mathbf{\Pi}\; dV \;=\; \mathbf{0} \;. \tag{0.12}$$

A corresponding relation can be established as

$$\int_{\mathcal{R}} \rho \boldsymbol{\pi}\; dv \;=\; \mathbf{0} \;, \tag{0.13}$$

where $\boldsymbol{\pi} = \mathbf{x} - \bar{\mathbf{x}}$ is the relative position vector in the current configuration. It follows that in the current configuration , the linear momentum $\mathbf{G}$ and the angular momentum $\mathbf{H}$ of the body relative to $\bar{\mathbf{x}}$, are

$$\mathbf{G} \;=\; \int_{\mathcal{R}} \rho \dot{\mathbf{x}}\; dv \;, \qquad \mathbf{H} \;=\; \int_{\mathcal{R}} \rho \boldsymbol{\pi} \times \dot{\boldsymbol{\pi}}\; dv \;, \tag{0.14}$$

respectively. Clearly, equations (12-14) are applicable to both deformable and rigid continua. Let the angular velocity tensor be defined as $\mathbf{\Omega} = \dot{\mathbf{Q}}\mathbf{Q}^T$ and note that the skew-symmetry of $\mathbf{\Omega}$ implies the existence of an axial (angular velocity) vector, such that $\mathbf{\Omega}\boldsymbol{\alpha} = \boldsymbol{\omega} \times \boldsymbol{\alpha}$, for any vector $\boldsymbol{\alpha}$. Using (8), it can be easily seen that

$$\boldsymbol{\pi} \;=\; \mathbf{Q}\mathbf{\Pi} \;, \quad \dot{\boldsymbol{\pi}} \;=\; \mathbf{\Omega}\, \boldsymbol{\pi} \;=\; \boldsymbol{\omega} \times \boldsymbol{\pi} \;, \quad \dot{\boldsymbol{\pi}} \cdot \boldsymbol{\pi} \;=\; 0 \;. \tag{0.15}$$

With the aid of $(14)_2$, the angular momentum $\mathbf{H}$ may be expressed as

$$\mathbf{H} \;=\; \mathbf{J}\boldsymbol{\omega} \;, \tag{0.16}$$

where the inertia tensor $\mathbf{J}$ is defined by

$$\mathbf{J} \;=\; \int_{\mathcal{R}} \rho \, \left((\boldsymbol{\pi} \cdot \boldsymbol{\pi}) \, \mathbf{I} \;-\; \boldsymbol{\pi} \otimes \boldsymbol{\pi} \right) \, dv \; . \tag{0.17}$$

The principles of linear and angular momentum are

$$\mathbf{f} \;=\; \dot{\mathbf{G}} \;=\; m \ddot{\mathbf{x}} \; , \quad \mathbf{M} \;=\; \dot{\mathbf{H}} \;=\; \dot{\mathbf{J}} \boldsymbol{\omega} \;+\; \mathbf{J} \dot{\boldsymbol{\omega}} \; , \tag{0.18}$$

where use has been made of equations (13-16). Note that in contrast with (6), equations (18) are *ordinary* differential equations.

0.2.3 Theory of Pseudo-rigid Bodies

Between the above two extremes represented by rigid and general deformable continua, one may consider bodies whose motion is governed by ordinary-differential equations (as with rigid bodies) and which are capable of undergoing certain restricted modes of deformation. Pseudo-rigid bodies fall within the above framework: they may undergo only homogeneous deformation. Recall that the motion of a general deformable body is defined by equation (1), hence the deformation gradient $\mathbf{F}$ is given by

$$d\mathbf{x} \;=\; \mathbf{F}(\mathbf{X}, t) \; d\mathbf{X} \; . \tag{0.19}$$

Since the deformation of a pseudo-rigid body is spatially homogeneous, the deformation gradient depends on time only, namely

$$d\mathbf{x} \;=\; \mathbf{F}(t) \; d\mathbf{X} \; , \tag{0.20}$$

or after integrating the above equation,

$$\mathbf{x} \;=\; \mathbf{F}(t)(\mathbf{X} \;-\; \bar{\mathbf{X}}) \;+\; \bar{\mathbf{x}} \; . \tag{0.21}$$

A purely mechanical theory, such as that for pseudo-rigid bodies, should be consistent with Euler's first and second law as they apply to general deformable continua. The equation of linear momentum balance for the pseudo-rigid bodies can be derived from equation (3) with the aid of the transport theorem as

$$\begin{aligned} \mathbf{f} \;&=\; \int_{\mathcal{R}} \rho \ddot{\mathbf{x}} \; dv \\ &=\; \int_{\mathcal{R}} \rho \; (\ddot{\bar{\mathbf{x}}} \;+\; \ddot{\boldsymbol{\pi}}) \; dv \\ &=\; m \ddot{\bar{\mathbf{x}}} \; . \end{aligned} \tag{0.22}$$

Indeed, the equation of linear momentum balance for the pseudo-rigid bodies is identical to the respective equation in rigid-body mechanics, in the form $(18)_1$.

Regarding angular momentum balance, note that by using (14), the tensor $\hat{\mathbf{H}}$ corresponding to the skew-symmetric part of angular momentum can be written as

$$\hat{\mathbf{H}} \;=\; \int_{\mathcal{R}} \rho\, (\dot{\boldsymbol{\pi}} \otimes \boldsymbol{\pi} \;-\; \boldsymbol{\pi} \otimes \dot{\boldsymbol{\pi}})\, dv \;. \tag{0.23}$$

By the definitions of $\boldsymbol{\Pi}$ and $\boldsymbol{\pi}$, it is seen from equation (8) that $\boldsymbol{\pi} = \mathbf{F}\boldsymbol{\Pi}$, so that equation (23) can be rewritten as

$$\hat{\mathbf{H}} \;=\; \int_{\mathcal{R}_o} \rho_o\, (\dot{\mathbf{F}}\boldsymbol{\Pi} \otimes \mathbf{F}\boldsymbol{\Pi} \;-\; \mathbf{F}\boldsymbol{\Pi} \otimes \dot{\mathbf{F}}\boldsymbol{\Pi})\, dV \;. \tag{0.24}$$

Since $\mathbf{F}$ is a function of time only, equation (24) takes the form

$$\hat{\mathbf{H}} \;=\; \dot{\mathbf{F}} \left(\int_{\mathcal{R}_o} \rho_o \boldsymbol{\Pi} \otimes \boldsymbol{\Pi}\, dV \right) \mathbf{F}^{\mathbf{T}} \;-\; \mathbf{F} \left(\int_{\mathcal{R}_o} \rho_o \boldsymbol{\Pi} \otimes \boldsymbol{\Pi}\, dV \right) \dot{\mathbf{F}}^{\mathbf{T}} \;. \tag{0.25}$$

Defining the Euler tensor $\mathbf{E}_o$ as,

$$\mathbf{E}_o \;=\; \int_{\mathcal{R}_o} \rho_o \boldsymbol{\Pi} \otimes \boldsymbol{\Pi}\, dV, \tag{0.26}$$

the tensor $\hat{\mathbf{H}}$ can be rewritten as

$$\hat{\mathbf{H}} \;=\; \dot{\mathbf{F}}\mathbf{E}_o\mathbf{F}^T \;-\; \mathbf{F}\mathbf{E}_o\dot{\mathbf{F}}^T \;. \tag{0.27}$$

Differentiating (27) with respect to time, one may deduce the skew-symmetric part of angular momentum balance in the form

$$\hat{\mathbf{M}} \;=\; \dot{\hat{\mathbf{H}}} \;=\; \ddot{\mathbf{F}}\mathbf{E}_o\mathbf{F}^T \;-\; \mathbf{F}\mathbf{E}_o\ddot{\mathbf{F}}^T \;. \tag{0.28}$$

Next, define the mean Cauchy stress tensor $\bar{\mathbf{T}}$ over the body as

$$V\bar{\mathbf{T}} \;=\; \int_{\mathcal{R}} \mathbf{T}\, dv \;, \tag{0.29}$$

or equivalently

$$2V\bar{\mathbf{T}} \;=\; \int_{\mathcal{R}} (\mathbf{T}\,\mathbf{I}^T \;+\; \mathbf{I}\,\mathbf{T}^T)\, dv \;, \tag{0.30}$$

where, using the definition of $\boldsymbol{\pi}$,

$$\mathbf{I} \;=\; \frac{\partial \boldsymbol{\pi}}{\partial \mathbf{x}} \;. \tag{0.31}$$

Using (6), (31) and invoking the divergence theorem, equation (30) leads to

$$\begin{aligned} 2V\bar{\mathbf{T}} \;&=\; \int_{\partial\mathcal{R}} (\mathbf{t}\otimes\boldsymbol{\pi} \;+\; \boldsymbol{\pi}\otimes\mathbf{t})\; da \;+\; \int_{\mathcal{R}} \rho\; (\mathbf{b}\otimes\boldsymbol{\pi} \;+\; \boldsymbol{\pi}\otimes\mathbf{b})\; dv \\ &-\; \int_{\mathcal{R}} \rho\; (\ddot{\mathbf{x}}\otimes\boldsymbol{\pi} \;+\; \boldsymbol{\pi}\otimes\ddot{\mathbf{x}})\; dv \;. \end{aligned} \tag{0.32}$$

Since $\boldsymbol{\pi} = \mathbf{F}\boldsymbol{\Pi},\ \mathbf{x} = \boldsymbol{\pi} + \bar{\mathbf{x}}$, it follows from (32) that

$$\begin{aligned} 2V\bar{\mathbf{T}} \;&=\; \int_{\partial\mathcal{R}} (\mathbf{t}\otimes\boldsymbol{\pi} \;+\; \boldsymbol{\pi}\otimes\mathbf{t})\; da \;+\; \int_{\mathcal{R}} \rho\; (\mathbf{b}\otimes\boldsymbol{\pi} \;+\; \boldsymbol{\pi}\otimes\mathbf{b})\; dv \\ &-\; \ddot{\mathbf{F}} \left(\int_{\mathcal{R}_o} \rho_o\, \boldsymbol{\Pi}\otimes\boldsymbol{\Pi}\; dV\right) \mathbf{F}^T \;-\; \mathbf{F} \left(\int_{\mathcal{R}_o} \rho_o\, \boldsymbol{\Pi}\otimes\boldsymbol{\Pi}\; dV\right) \ddot{\mathbf{F}}^T \\ &-\; \int_{\mathcal{R}} \rho\; (\ddot{\bar{\mathbf{x}}}\otimes\boldsymbol{\pi} + \boldsymbol{\pi}\otimes\ddot{\bar{\mathbf{x}}})\; dv \;. \end{aligned} \tag{0.33}$$

With the aid of (13), it can be shown that the last term of the above equation vanishes identically. Using (26), it may be concluded that

$$\begin{aligned} 2V\bar{\mathbf{T}} \;&=\; \int_{\partial\mathcal{R}} (\mathbf{t}\otimes\boldsymbol{\pi} \;+\; \boldsymbol{\pi}\otimes\mathbf{t})\; da \;+\; \int_{\mathcal{R}} \rho\; (\mathbf{b}\otimes\boldsymbol{\pi} \;+\; \boldsymbol{\pi}\otimes\mathbf{b})\; dv \\ &-\; \ddot{\mathbf{F}}\mathbf{E}_o\mathbf{F}^T \;-\; \mathbf{F}\mathbf{E}_o\ddot{\mathbf{F}}^T \;, \end{aligned} \tag{0.34}$$

which constitutes the symmetric part of angular momentum balance. From (22), (28) and (34), it is seen that the equations of motion for a pseudo-rigid body are ordinary differential equations.

Instead of the local Cauchy stress tensor field $\mathbf{T}$ used in general deformable continua, pseudo-rigid bodies sustain only a mean or average Cauchy stress tensor $\bar{\mathbf{T}}$, acting uniformly throughout the domain of the body. Consequently, local constitutive equations of the form $\mathbf{T} = \hat{\mathbf{T}}(\mathbf{X}, \mathbf{F})$ postulated for general continua give way to global constitutive equations $\bar{\mathbf{T}} = \hat{\mathbf{T}}(\mathbf{F})$. If the body $\mathcal{B}$ is composed of Green-elastic material, then there exists a strain energy ε per unit mass, such that

$$\mathbf{S} = \rho_o \frac{\partial \varepsilon}{\partial \mathbf{E}} \;, \tag{0.35}$$

where $\mathbf{S}$ is the second Piola-Kirchhoff stress tensor and $\mathbf{E} = \frac{1}{2}(\mathbf{F}^T\mathbf{F} - \mathbf{I})$ is the relative Lagrangian strain tensor. For example, assuming that the material produces a neo-Hookean response,

$$\rho_o \varepsilon = \mu \ \mathrm{tr}\mathbf{E} \ , \tag{0.36}$$

where $\mu > 0$ is a material constant. In view of (35), it is concluded that

$$\mathbf{S} = \mu \mathbf{I} \, . \tag{0.37}$$

Recalling that the Cauchy stress tensor $\mathbf{T}$ and the second Piola-Kirchhoff stress tensor $\mathbf{S}$ are related according to

$$J\mathbf{T} = \mathbf{F}\mathbf{S}\mathbf{F}^T \ , \tag{0.38}$$

the constitutive law (37) can be expressed in the form

$$\bar{\mathbf{T}} = \mu \mathbf{B} \ , \tag{0.39}$$

where $\mathbf{B} = \mathbf{F}\mathbf{F}^T$ is the left Cauchy-Green deformation tensor.

The theory of pseudo-rigid bodies provides a convenient framework, much like classical rigid-body mechanics, for the analysis of changes in the position and orientation of a body subjected to external loading. In particular, it represents a generalization of rigid-body mechanics. At the same time, the theory of pseudo-rigid bodies is capable of predicting gross deformation and associated stresses. In that sense, it represents a restriction, or a "coarse" version, of the theory of elasticity.

0.2.4 Theory of a Cosserat Point

In the previous report [19], the theory of a Cosserat point was used to establish the vehicle model. We find it appropriate to outline the correspondence between this theory and the theory of pseudo-rigid bodies here. Several of these results are seemingly well known; indeed they can be inferred from Cohen and Muncaster's earlier work [10].

We recall that a Cosserat point is a theoretical model for a continuum. The present configuration of the Cosserat point is defined by the vectors $\mathbf{r}$ and $\mathbf{d}_N$, which are vector-valued functions of time. The latter vectors are known as directors. For the present purposes, N is a free index which has a range from 1 to K, where K is the number of directors. Corresponding to

these vectors, we define a fixed reference configuration of the Cosserat point by the constant vectors $\mathbf{R}$ and $\mathbf{D}_N$. The velocity and director velocities of the Cosserat point are

$$\mathbf{v} = \dot{\mathbf{r}} \quad , \quad \mathbf{w}_N = \dot{\mathbf{d}}_N \quad , \quad N = 1, \ldots, K \quad , \tag{0.40}$$

where a superposed dot denotes the time derivative.

From the developments of Rubin [21] and Green and Naghdi [12], we recall the mass conservations, the balance of linear momentum, the K balances of director momentum and the balance of angular momentum:

$$\dot{m} = 0 \quad , \quad \dot{y}^N = 0 \quad , \quad \dot{y}^{MN} = 0 \quad , \tag{0.41}$$

$$m(\dot{\mathbf{v}} + y^N \dot{\mathbf{w}}_N) = \mathbf{n} \quad , \tag{0.42}$$

$$m(y^N \dot{\mathbf{v}} + y^{NM} \dot{\mathbf{w}}_M) = \mathbf{l}^N - \mathbf{k}^N \quad , \tag{0.43}$$

$$\mathbf{d}_N \times \mathbf{k}^N = \mathbf{0} \quad . \tag{0.44}$$

In these equations, m is the mass of the Cosserat point, y^N, $y^{NM} = y^{MN}$ are its inertia parameters, $\mathbf{n}$ is the applied force, $\mathbf{l}^N$ are the applied director forces and $\mathbf{k}^N$ are the intrinsic director forces.

To establish a correspondence between the two theories, it is first necessary to assume that K, the number of directors, is 3. It is assumed that the inertia coefficients y^N are zero. We next define the following invertible tensor:

$$\mathbf{F} = \mathbf{d}_i \otimes \mathbf{D}^i \quad . \tag{0.45}$$

where $\mathbf{D}^i = \delta^i_k \mathbf{D}_k$ and δ^i_k is the Kronecker delta. Subsequently the two Euler tensors for the pseudo-rigid body can be defined in terms of the directors using the identities

$$\mathbf{E}_0 = m y^{ik}\, \mathbf{D}_i \otimes \mathbf{D}_i \quad , \quad \mathbf{E} = m y^{ik}\, \mathbf{d}_i \otimes \mathbf{d}_i \quad . \tag{0.46}$$

The two final identifications concern the forces. First,

$$V\bar{\mathbf{T}} = \mathbf{k}^i \otimes \mathbf{d}_i \quad . \tag{0.47}$$

Then, the assigned forces are identified with the surface traction and body force contributions to the left hand side of the balance of angular momentum for the pseudo-rigid body (see equation (34)). With the aid of some elementary calculations, it may be shown that the solutions to the equations governing the motion of the pseudo-rigid body will be identical to those obtained using the corresponding equations for a Cosserat point.

0.3 Impact of Two Pseudo-rigid Bodies

The kinematic constraints imposed on contacting bodies is of utmost importance in the analysis of vehicular collision. In this section, contact is considered by constructing a simplified vehicle geometry, by detecting potential collisions, and by numerically finding the location of the contact and the direction of contact forces.

The dynamic contact problem distinguishes itself from its static counterpart in that the inequality constraint conditions stemming from impenetrability hold not only for the displacements along the contacting surfaces but also for their time rates. The impenetrability constraint [26] may be expressed in equality form during persistent contact as

$$[(\mathbf{X}_2 + \mathbf{u}_2) - (\mathbf{X}_1 + \mathbf{u}_1)] \cdot \mathbf{n}_1(\mathbf{X}, t) = 0 , \tag{0.48}$$

where $\mathbf{u}_1 = \mathbf{u}_1(\mathbf{X}_1, t)$, $\mathbf{u}_2 = \mathbf{u}_2(\mathbf{X}_2, t)$ are the displacements for bodies $\mathcal{B}_1$ and $\mathcal{B}_2$ and $\mathbf{n}_1$ is the smooth outward unit normal to the boundary $\partial\mathcal{R}_1$ of $\mathcal{B}_1$ in the current configuration. The material time derivative of (48) results in

$$(\dot{\mathbf{u}}_2 - \dot{\mathbf{u}}_1) \cdot \mathbf{n}_1 + [(\mathbf{X}_2 + \mathbf{u}_2) - (\mathbf{X}_1 + \mathbf{u}_1)] \cdot \dot{\mathbf{n}}_1 = 0 . \tag{0.49}$$

Taking into account that the unit normal $\mathbf{n}_1$ lies in the direction of the vector connecting the contacting points, it can be readily shown that

$$[(\mathbf{X}_2 + \mathbf{u}_2) - (\mathbf{X}_1 + \mathbf{u}_1)] \cdot \dot{\mathbf{n}}_1 = 0 . \tag{0.50}$$

This, in turn, implies that (49) reduces to

$$(\dot{\mathbf{u}}_2 - \dot{\mathbf{u}}_1) \cdot \mathbf{n}_1 = 0 . \tag{0.51}$$

In the context of this work, the vehicle is approximated by an ellipsoid and modeled as a three dimensional pseudo-rigid body as shown in Figure 3, where A, B and C are principal semi-axes of the ellipsoid. Consequently, a typical vehicle consists of main body whose surface is approximated by an ellipsoidal, in addition to the suspensions and the tyres, as discussed in [19]. The choice of ellipsoidals greatly simplifies the ensuing computations and provides a geometric description which is consistent in its level of approximation with kinematic assumption of spatially homogeneous deformation, as

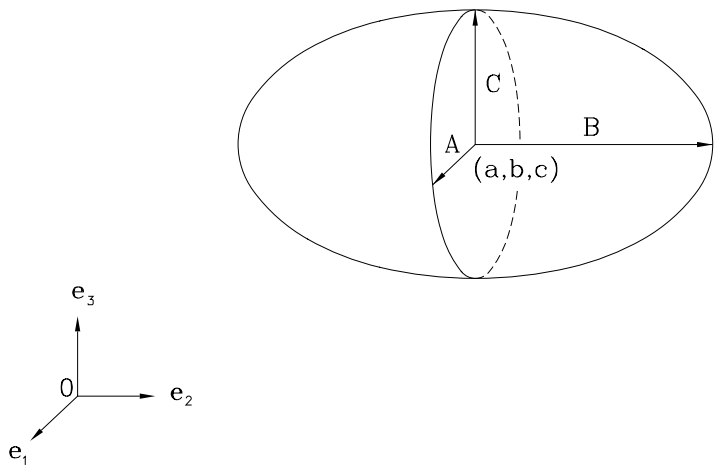

Figure 0.3: The representation of an ellipsoid in Cartesian coordinates.

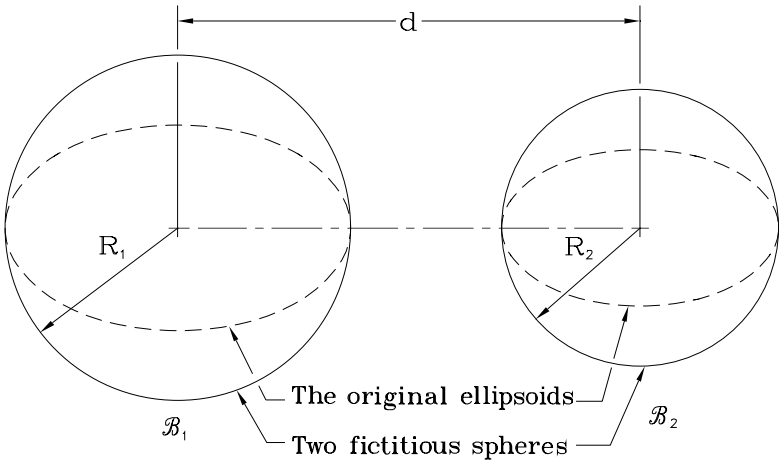

Figure 0.4: The detection of potential contact.

stated in equation (21). Clearly, the high-order surfaces can be considered, preferably in connection with the admittance of non-homogeneous deformations.

The impact history is identified by distinct stages, namely, (i) pre-impact, (ii) impact and (iii) post-impact. In order to provide a crude check of potential contact, the two ellipsoids are superscribed by fictitious spheres, as shown in Figure 4 in the spirit of well-known pin-ball algorithm [2]. Subsequently, the equations of motion are advanced in time using a higher-order accurate Runge-Kutta integration scheme discussed in the companion report [19]. At each discrete time, contact between the two vehicles is checked using the condition

$$d \;\leq\; R_1 \;+\; R_2 \;, \tag{0.52}$$

where d is the distance between the mass centers of $\mathcal{B}_1$ and $\mathcal{B}_2$ in the current configuration and the radii of two fictitious spheres, R_1 and R_2, are the maximum principal semi-axes of the two ellipsoids, respectively.

If (52) holds, then two vehicles are in *potential* contact. Since the time steps used in the simulation are generally small, the penetration region (if it exists) can be reasonably well approximated by a point, which is referred to as the contact point. Once the two bodies are in potential contact, the analysis focuses on the exact ellipsoidal geometries. This approach is particularly important from the standpoint of computational efficiency, as it permits a "fast" check of potential contact without resorting to the exact geometries of the bodies.

The equation of an ellipsoid along its principal axes is

$$\frac{(x_1 - a)^2}{A^2} \;+\; \frac{(x_2 - b)^2}{B^2} \;+\; \frac{(x_3 - c)^2}{C^2} \;=\; 1 \;, \tag{0.53}$$

where a, b and c represent the position of center of mass of ellipsoid with respect to the Cartesian coordinate system with basis vectors $\mathbf{e}_1$, $\mathbf{e}_2$ and $\mathbf{e}_3$, as shown in Figure 3, and $\mathbf{x} \;=\; x_i \mathbf{e}_i$.

A point on the surface of the ellipsoid can also be represented parametrically [15] by its position vector as

$$\begin{aligned} \mathbf{R} \;&=\; (a \;+\; A\;\cos u\;\cos v)\;\mathbf{e}_1 \;+\; (b \;+\; B\;\cos u\;\sin v)\;\mathbf{e}_2 \\ &+\; (c \;+\; C\;\sin u)\;\mathbf{e}_3 \;, \end{aligned} \tag{0.54}$$

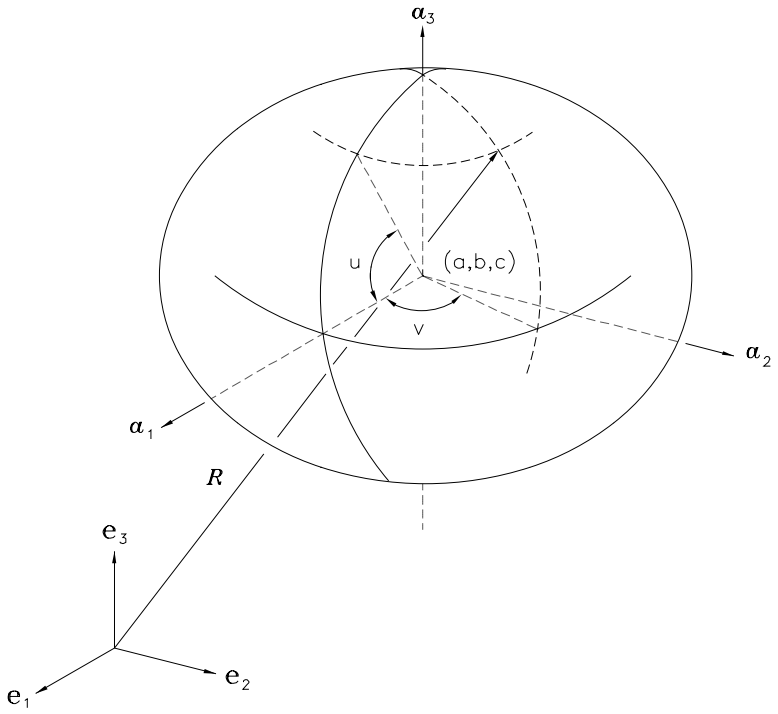

Figure 0.5: Parametric representation of an ellipsoid.

where $u \in [-\pi/2, \pi/2]$, $v \in [0, 2\pi]$ are the surface coordinates of the ellipsoid and $\mathbf{a}_i$ $(i = 1, 2, 3)$ lie in the principal directions of ellipsoid (cf. Figure 5). Thus, the parametric representation of two bodies can be expressed as

$$\begin{aligned} \mathbf{R}_1 &= (a_1 + A_1 \cos u_1 \cos v_1)\, \mathbf{e}_1 + (b_1 + B_1 \cos u_1 \sin v_1)\, \mathbf{e}_2 \\ &+ (c_1 + C_1 \sin u_1)\, \mathbf{e}_3 \,, \end{aligned} \tag{0.55}$$

and

$$\begin{aligned} \mathbf{R}_2 &= (a_2 + A_2 \cos u_2 \cos v_2)\, \mathbf{e}'_1 + (b_2 + B_2 \cos u_2 \sin v_2)\, \mathbf{e}'_2 \\ &+ (c_2 + C_2 \sin u_2)\, \mathbf{e}'_3 \,. \end{aligned} \tag{0.56}$$

where $\mathbf{e}_i$, $i = 1, 2, 3$, are the principal directions of $\mathcal{B}_1$ and $\mathbf{e}'_i$ are the principal directions of $\mathcal{B}_2$ in the reference configuration.

Next, introduce a rotation tensor $\mathbf{Q}$ that requires three parameters for its specification. Euler provided a very clear way of constructing $\mathbf{Q}$ as three

simple rotations, according to which

$$\mathbf{e}_i \;=\; \mathbf{Q}(\phi)\mathbf{Q}(\theta)\mathbf{Q}(\psi)\mathbf{E}_i \;=\; \mathbf{Q}\mathbf{E}_i \;,\quad (i=1,2,3)\;, \tag{0.57}$$

where $\mathbf{Q} \;=\; Q_ij\mathbf{E_i}\otimes\mathbf{E_j}$ and

$$\left(\; Q_{ij} \;\right) = \begin{pmatrix} \cos\theta\cos\psi & \cos\theta\sin\psi & -\sin\theta \\ \sin\phi\sin\theta\cos\psi - \cos\phi\sin\psi & \sin\phi\sin\theta\sin\psi + \cos\phi\cos\psi & \sin\phi\cos\theta \\ \cos\phi\sin\theta\cos\psi + \sin\phi\sin\psi & \cos\phi\sin\theta\sin\psi - \sin\phi\cos\psi & \cos\phi\cos\theta \end{pmatrix}. \tag{0.58}$$

The angles ϕ, θ and ψ are known as the Euler angles (see, for example, [14]) and $\mathbf{E}_i$ are the basis vectors of a fixed orthonormal basis.

Given the above setting, the equations of the two bodies (55) and (56) can be referred to a common basis $\mathbf{E}_i$ whose origin is attached to the center of mass of $\mathcal{B}_1$ and which translates, but does not rotate, with $\mathcal{B}_1$. We choose the initial configuration as the reference configuration of two bodies and consider the Euler angles, the positions of mass center and the principal semi-axes for the $\mathcal{B}_1$ and $\mathcal{B}_2$ as the initial conditions of the vehicular impact simulation system.

The reference configuration of two ellipsoids are

$$\mathbf{R}_1 \;=\; X_1(u_1,v_1)\;\mathbf{E}_1 \;+\; Y_1(u_1,v_1)\;\mathbf{E}_2 \;+\; Z_1(u_1,v_1)\;\mathbf{E}_3\;, \tag{0.59}$$

$$\mathbf{R}_2 \;=\; X_2(u_2,v_2)\;\mathbf{E}_1 \;+\; Y_2(u_2,v_2)\;\mathbf{E}_2 \;+\; Z_2(u_2,v_2)\;\mathbf{E}_3\;. \tag{0.60}$$

Clearly, $\mathbf{R}_1$ and $\mathbf{R}_2$ are functions of u_1, v_1, and u_2, v_2 in their respective reference configurations.

Given that both bodies are modeled as pseudo-rigid, it follows from (21) that

$$\mathbf{x}_1 \;=\; \mathbf{F}_1\;(\mathbf{X}_1 \;-\; \bar{\mathbf{X}}_1) \;+\; \bar{\mathbf{x}}_1\;, \tag{0.61}$$

$$\mathbf{x}_2 \;=\; \mathbf{F}_2\;(\mathbf{X}_2 \;-\; \bar{\mathbf{X}}_2) \;+\; \bar{\mathbf{x}}_2\;, \tag{0.62}$$

where $\mathbf{F}_1(t)$ and $\mathbf{F}_2(t)$ are the deformation gradients for $\mathcal{B}_1$ and $\mathcal{B}_2$, respectively. Since the common basis is attached to, and translates with, the center of mass of $\mathcal{B}_1$, $\bar{\mathbf{X}}_1$ and $\bar{\mathbf{x}}_1$ vanish identically. In addition, $\bar{\mathbf{X}}_2$ is given by the

initial conditions, while $\bar{\mathbf{x}}_2$ is function of time only. Using (59-62), the surfaces of $\mathcal{B}_1$ and $\mathcal{B}_2$ are respectively parametrized in the present configurations as

$$\mathbf{r}_1 \;=\; x_1(u_1, v_1)\;\mathbf{E}_1 \;+\; y_1(u_1, v_1)\;\mathbf{E}_2 \;+\; z_1(u_1, v_1)\;\mathbf{E}_3\;, \tag{0.63}$$

$$\mathbf{r}_2 \;=\; x_2(u_2, v_2)\;\mathbf{E}_1 \;+\; y_2(u_2, v_2)\;\mathbf{E}_2 \;+\; z_2(u_2, v_2)\;\mathbf{E}_3\;, \tag{0.64}$$

where $\mathbf{r}_1$ and $\mathbf{r}_2$ are the position vectors in the current configuration.

The points of potential contact on the two surfaces are defined so that the distance $\mathcal{S}$ between them,

$$S(u_1, v_1, u_2, v_2) \;=\; ||\mathbf{r}_1 - \mathbf{r}_2||\;, \tag{0.65}$$

attains a minimum. The extrema of $\mathcal{S}$ are found by solving the system of non-linear algebraic equation

$$\frac{\partial S}{\partial u_1} \;=\; 0 \quad , \quad \frac{\partial S}{\partial v_1} \;=\; 0 \quad , \quad \frac{\partial S}{\partial u_2} \;=\; 0 \quad , \quad \frac{\partial S}{\partial v_2} \;=\; 0\;, \tag{0.66}$$

numerically.

After determining the values of u_1, v_1, u_2 and v_2 corresponding to surface points which render $\mathcal{S}$ minimum, one can easily obtain

$$\mathbf{a}_{u1} \;=\; \frac{\partial \mathbf{r}_1}{\partial u_1} \quad , \quad \mathbf{a}_{v1} \;=\; \frac{\partial \mathbf{r}_1}{\partial v_1} \quad , \quad \mathbf{a}_{u2} \;=\; \frac{\partial \mathbf{r}_2}{\partial u_2} \quad , \quad \mathbf{a}_{v2} \;=\; \frac{\partial \mathbf{r}_2}{\partial v_2}\;, \tag{0.67}$$

where $\mathbf{a}_{u1},\ \mathbf{a}_{v1},\ \mathbf{a}_{u2},\ and\ \mathbf{a}_{v2}$ are the tangent vectors at the potential contact points along the coordinate curves $u = u_1, v = v_1, u = u_2$ and $v = v_2$ on the surfaces of $\mathcal{B}_1$ and $\mathcal{B}_2$ in their current configurations. The corresponding unit outward normal vectors $\mathbf{n}_1\ and\ \mathbf{n}_2$ are

$$\mathbf{n}_1 \;=\; \frac{\mathbf{a}_{v1} \times \mathbf{a}_{u1}}{||\mathbf{a}_{v1} \times \mathbf{a}_{u1}||}\;, \tag{0.68}$$

$$\mathbf{n}_2 \;=\; \frac{\mathbf{a}_{v2} \times \mathbf{a}_{u2}}{||\mathbf{a}_{v2} \times \mathbf{a}_{u2}||}\;. \tag{0.69}$$

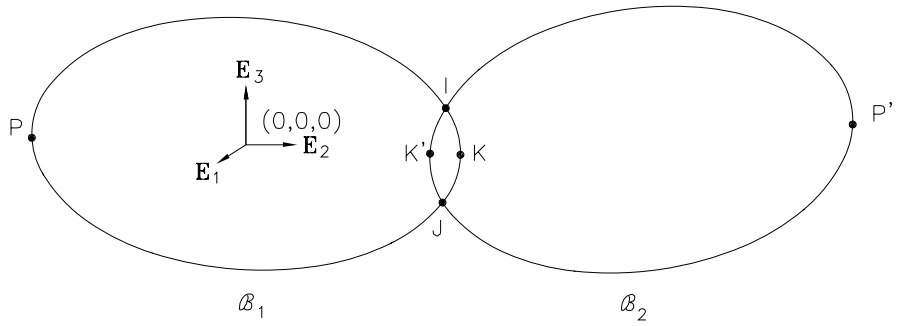

Figure 0.6: The locations of possible contact points.

At this stage, contact penetration of the two surface points can be checked using

$$(\mathbf{r_2} - \mathbf{r_1}) \cdot \mathbf{n_1} \leq 0 \ . \tag{0.70}$$

Given the ellipsoidal geometry of the two bodies, equations (66) may converge to a set of solution for u_1, v_1, u_2 and v_2 that corresponds to pairs of points such as I-I, J-J, K-K′, P-K′ and K-P′, as shown in Figure 6. Typically, equations (66) are solved using an iterative scheme such as Newton's method (cf. [1], [20] and [16]), where the solution which is obtained depends critically on the initial guess for u_1, v_1, u_2 and v_2. An appropriate pair of contact points can be identified by checking the corresponding distance $\mathcal{S}$. Since only I-I, J-J and K-K′ are valid pairs of contact points, the criterion

$$S \ < \ \min \ (\mathrm{A}_1, \ \mathrm{B}_1, \ \mathrm{C}_1, \ \mathrm{A}_2, \ \mathrm{B}_2, \ \mathrm{C}_2) \ , \tag{0.71}$$

can be used to filter out the pairs P-K′ and K-P′. One may then substitute the solution into (63) and (64) to obtain the position vector of the contact points. As argued previously, since the time step Δt is small any one of the remaining solutions is considered valid to within an error of order Δt.

0.4 Illustrative Examples

The implementation of the impact algorithm between two pseudo-rigid ellipsoidal bodies was conducted using *Mathematica* [29]. The relevant files are available on request by contacting the authors at oreilly@me.berkeley.edu or

panos@me.berkeley.edu. In the sequel, four cases are presented. The first two cases verify that the algorithm could detect the contact points of two bodies. The remaining two cases show how the algorithm can be used to examine the pre-collision and post-collision motions of two colliding vehicles. These examples are clearly not exhaustive of the capabilities of the algorithm and are intended for the purpose of illustration.

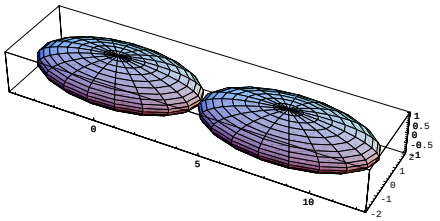

Figure 0.7: Head-to-head contact of two vehicles.

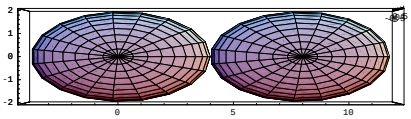

Figure 0.8: Top view of the head-to-head contact of two vehicles.

The first case, which is shown in Figures 7 and 8, is a head-to-head contact of two ellipsoids. The principal semi-axes for two ellipsoids are

$$A_1 \;=\; 4.0\;(m) \quad , \quad B_1 \;=\; 2.0\;(m) \quad , \quad C_1 \;=\; 1.0\;(m)\;, \tag{0.72}$$

$$A_2 \;=\; 4.0\;(m) \quad , \quad B_2 \;=\; 2.0\;(m) \quad , \quad C_2 \;=\; 1.0\;(m)\;. \tag{0.73}$$

In this case, the rotation tensors of the two ellipsoids are identity tensors. The position of the geometric center of ellipsoid 1 is at origin and that of ellipsoid 2 is

$$\bar{\mathbf{x}}_2 \;=\; 8\mathbf{E}_1\;. \tag{0.74}$$

As expected, the algorithm predicted the correct contact point and unit outward normal vectors at the contact points (cf. Figure 8).

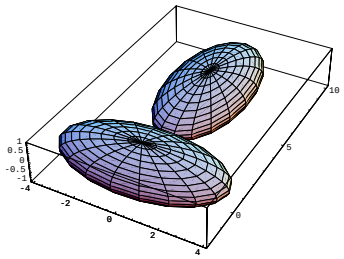

Figure 0.9: Head-to-side contact of two vehicles.

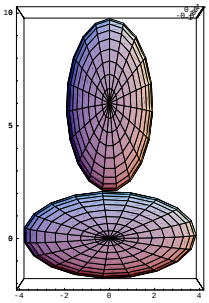

Figure 0.10: Top view of the head-to-side contact of two vehicles.

The detection of the position vectors of the contact points and the unit outward normal vectors at the contact points for the head-to-side contact of two vehicles is the second case considered (cf. Figures 9 and 10). The Euler angle ψ was changed to $\pi/2$ from the previous example, and the position vector of the geometric center of ellipsoid 2 was changed to (0,6,0). The other parameters remained the same. As expected, the algorithm predicted the correct results.

A sequence of graphics, shown in Figure 11, shows the pre-collision, collision and post-collision of two vehicles for a specific set of initial conditions. The two vehicles in this, the third, example initially move with velocities

$$\mathbf{v}_1 \;=\; 25\;\mathbf{E}_1\;(km/h) \quad , \quad \mathbf{v}_2 \;=\; 20\;\mathbf{E}_1\;(km/h)\;. \tag{0.75}$$

In this situation, the vehicle model described in [19] is used to simulate the behavior of ellipsoid 1. The other ellipsoid is, again, assumed to be rigid and its motion unaffected by the collision. The principal semi-axes for the two

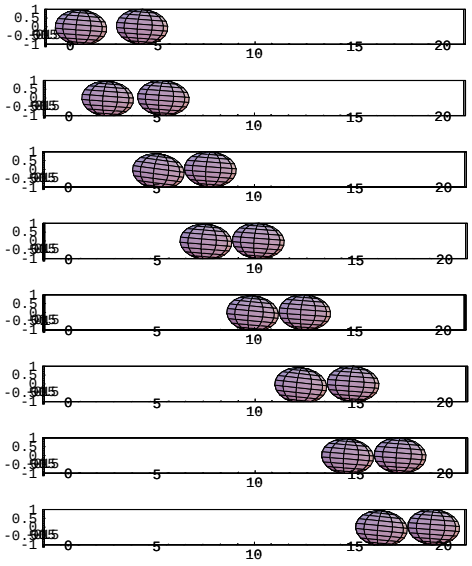

Figure 0.11: Side view of the pre-collision, collision and post-collision of two vehicles in a head-to-tail collision.

ellipsoids are

$$A_1 \;=\; 1.5\;(m) \quad , \quad B_1 \;=\; 1.0\;(m) \quad , \quad C_1 \;=\; 1.0\;(m)\;, \tag{0.76}$$

$$A_2 \;=\; 1.5\;(m) \quad , \quad B_2 \;=\; 1.0\;(m) \quad , \quad C_2 \;=\; 1.0\;(m)\;. \tag{0.77}$$

The position vectors of the center of mass of two ellipsoids at t = 0 are, respectively,

$$\bar{\mathbf{x}}_1 \;=\; -\,0.0406\mathbf{E}_3 \quad , \quad \bar{\mathbf{x}}_2 \;=\; 3.5\mathbf{E}_1\;. \tag{0.78}$$

The initial deformation gradients for body bodies are

$$\begin{aligned}\mathbf{F}_1(0) \;&=\; .9972\;(\mathbf{E}_1\otimes\mathbf{E}_1 \;+\; \mathbf{E}_3\otimes\mathbf{E}_3) \;-\; .0749(\mathbf{E}_1\otimes\mathbf{E}_3 \;-\; \mathbf{E}_3\otimes\mathbf{E}_1)\\ &+\; \mathbf{E}_2\otimes\mathbf{E}_2\;,\end{aligned} \tag{0.79}$$

$$\mathbf{F}_2(0) \;=\; \mathbf{E}_1\otimes\mathbf{E}_1 \;+\; \mathbf{E}_2\otimes\mathbf{E}_2 \;+\; \mathbf{E}_3\otimes\mathbf{E}_3\;. \tag{0.80}$$

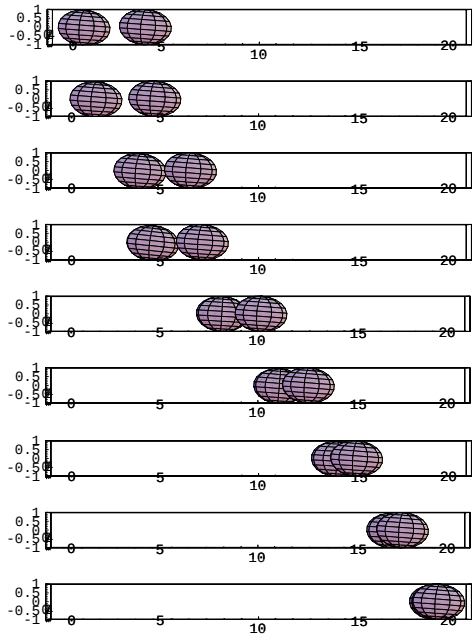

Figure 0.12: Side view of the pre-collision, collision and post-collision behavior of two vehicles which are involved in a head-to-tail collision with an initial 0.5 meter deviation.

The numerical simulation data is adopted from the companion report [19] and the results are shown in Figure 11. In this simulation, as expected, the velocity of the first body, which is deformable, is altered by the collision.

In the final case, all parameters are the same as previous case except that the position vector of the center of mass of the first ellipsoid was shifted to

$$\bar{\mathbf{x}}_1 \;=\; 0.5\mathbf{E}_2 \;-\; 0.0406\mathbf{E}_3 \;. \tag{0.81}$$

The motions of two vehicles in this impact scenario are shown in Figures 12 and 13.

0.5 Concluding Comments

In this report, the development and application of an algorithm to detect the possible collisions between two pseudo-rigid bodies was outlined. As pseudo-rigid bodies, and equivalent Cosserat points, were used to develop a vehicle

model in the precursor to this report [19], the proposed algorithm can be used in conjunction with this vehicle model. In this respect, the algorithm is a principal component of a model which is capable of modeling platoons of vehicles. We intend in subsequent reports to use the algorithm presented here in this manner.

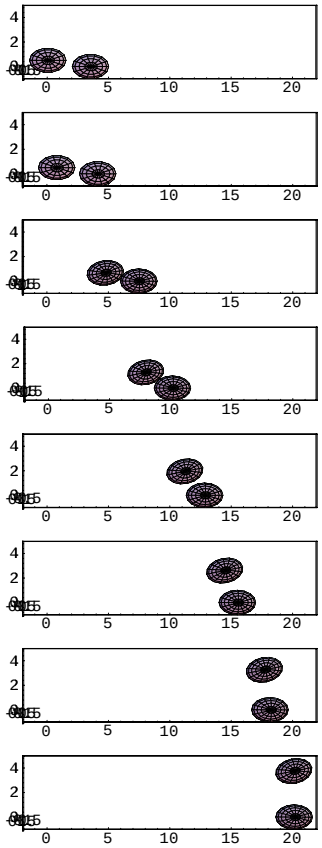

Figure 0.13: Top view of the pre-collision, collision and post-collision behavior of two vehicles which are involved in a head-to-tail collision with an initial 0.5 meter deviation.

Bibliography

[1] K. E. Atkinson. *An Introduction to Numerical Analysis*. 2nd edn., Wiley, New York, 1988.

[2] T. Belytschko. Contact-Impact by the Pinball Algorithm with Penalty and Lagrangian Methods. *International Journal for Numerical Methods in Engineering*, Vol. 31, pp. 547-572, 1991.

[3] J. Casey. A Treatment of Rigid Body Dynamics. *ASME Journal of Applied Mechanics*, Vol. 50, pp. 905-907, 1983 and Errata, Vol. 51, p. 227, 1984.

[4] J. Casey. On the Advantages of a Geometrical Viewpoint in the Derivation of Lagrange's Equations for a Rigid Continuum. *Journal of Applied Mathematics and Physics (ZAMP)*, Vol. 46 (Special Issue), pp. 805-847, 1995.

[5] J. Casey and V. C. Lam. On the Relative Angular Velocity Tensor. *ASME Journal of Mechanisms, Transmission and Automation in Design*, Vol. 108, pp. 399-400, 1986.

[6] H. Cohen. Pseudo-rigid Bodies. *Ultilitas Mathematica* Vol. 20, pp. 221-247, 1981.

[7] H. Cohen and G. P. Mac Sithigh. Impulsive Motions of Elastic Pseudo-rigid Bodies. *ASME Journal of Applied Mech.*, Vol. 58, pp. 1042-1048, 1991.

[8] H. Cohen and G. P. Mac Sithigh. Impulsive Motions of Elastic Pseudo-rigid Bodies II. *Journal of Elasticity*, Vol. 34, pp. 149-166, 1994.

[9] H. Cohen and G. P. Mac Sithigh. Plane Motions of Elastic Pseudo-rigid Bodies. *Journal of Elasticity*, Vol. 21, pp. 193-226, 1989.

[10] H. Cohen and R. G. Muncaster. *The Theory of Pseudo-Rigid Bodies.* Springer Tracts in Natural Philosophy, Vol. 33, Springer-Verlag, New York, 1988.

[11] S. M. Calso, N. K. Saha, M. O. Faruque, and K. S. Balabhadra. Simulation of Offset and In-Line Car to Car Rear Impacts. *Crashworthiness and Occupant Protection in Transportation Systems*, pp. 149-160, 1993.

[12] A. E. Green and P. M. Naghdi. A Thermomechanical Theory of a Cosserat Point with Application to Composite Materials. *Quarterly Journal of Mechanics and Applied Mathematics*, Vol. 44, pp. 335-355, 1991.

[13] A. E. Green and P. M. Naghdi. A Unified Procedure for Construction of Theories of Deformable Media. II: Generalized Continua. *Proceedings of the Royal Society of London, Series A*, Vol. 448, pp. 357-377, 1995.

[14] D. T. Greenwood. *Principles of Dynamics.* 2nd edn., Prentice Hall, New Jersey, 1988.

[15] E. Kreyszig. *Advanced Engineering Mathematics.* 6th edn., Wiley, New York, 1988.

[16] B. W. Kernighan and D. M. Ritchie. *The C Programming Language.* 2nd edn., Prentice Hall, New Jersey, 1988.

[17] C. G. Liang. Hierarchical Symbolic Vehicle Modeling Process: Multibody Dynamics and Order Reduction. *Advanced Automotive Technologies*, Vol. 13, pp. 177-184, 1989.

[18] L. E. Malvern. *Introduction to the Mechanics of a Continuous Medium.* Prentice Hall, New Jersey, 1969.

[19] O. M. O'Reilly, P. Papadopoulos, G. J. Lo and P. C. Varadi. *Models of Vehicular Collision: Development and Simulation with Emphasis on Safety, I: Development of a Model for a Single Vehicle.* UCB-ITS-PRR-97-18.

[20] W. H. Press, S. A. Teukolsky, W. T. Vetterling and B. P. Flannery. *Numerical Recipes in C: the Art of Scientific Computing.* 2nd edn., Cambridge University Press, Cambridge, 1992.

[21] M. B. Rubin. On the Theory of a Cosserat Point and its Application to the Numerical Solution of Continuum Problems. *ASME Journal of Applied Mechanics*, Vol. 52, pp. 368-372, 1985.

[22] M. B. Rubin. On the Numerical Solution of One-Dimensional Continuum Problems Using the Theory of a Cosserat Point. *ASME Journal of Applied Mechanics*, Vol. 52, pp. 373-378, 1985.

[23] J. J. Slawianowski. Analytical Mechanics of Finite Homogeneous Strains. *Archives of Mechanics*, Vol. 26, pp. 569-587, 1974.

[24] J. J. Slawianowski. Newtonian Dynamics of Homogeneous Strains. *Archives of Mechanics*, Vol. 27, pp. 93-102, 1975.

[25] J. J. Slawianowski. The Mechanics of the Homogeneously–Deformable Body. Dynamical Models with High Symmetries. *Zeitschrift für angewandte Mathematik und Mechanik (ZAMM)*, Vol. 62, pp. 229-240, 1982.

[26] R. L. Taylor and P. Papadopoulos. On a Finite Element Method for Dynamic Contact/Impact Problems. *International Journal for Numerical Methods in Engineering*, Vol. 36, pp. 2123-2140, 1993.

[27] B. D. Walker, J. C. Miles and T. J. Keer. Vehicle Crashworthiness from lumped Parameter to Continuum Models. *Crashworthiness and Occupant Protection in Transportation Systems*, pp. 67-74, 1993.

[28] E. T. Whittaker. *A Treatise on the Analytical Dynamics of Particles and Rigid Bodies*. 4th edn., Cambridge University Press, Cambridge, 1937.

[29] S. Wolfram. *Mathematica: A System for Doing Mathematics by Computer*. 2nd edn., Addison-Wesley, California, 1991.